

## Article

# Wound Coating Collagen-Based Composites with Ag Nanoparticles: Synthesis, Structure and Biological Activity

Alexander Vasil'kov <sup>1</sup>, Natalya Tseomashko <sup>2,\*</sup>, Anastasia Tretyakova <sup>1</sup>, Aziza Abidova <sup>2</sup>, Ivan Butenko <sup>1,3</sup>, Alexander Pereyaslvtsev <sup>4</sup>, Natalia Arkharova <sup>5</sup>, Vladimir Volkov <sup>5</sup> and Eleonora Shtykova <sup>5</sup>

<sup>1</sup> A.N. Nesmeyanov Institute of Organoelement Compounds, RAS, 119991 Moscow, Russia; alexandervasilkov@yandex.ru (A.V.); anastasia.n.tretyakova@gmail.com (A.T.); solmaersgold@gmail.com (I.B.)

<sup>2</sup> Department of Interuniversity Research Laboratory, Tashkent Medical Academy, Tashkent 100109, Uzbekistan; azizka32@inbox.ru

<sup>3</sup> G.F. Gause Institute of New Antibiotics, 119021 Moscow, Russia

<sup>4</sup> Dukhov Automatics Research Institute, 127030 Moscow, Russia; pereaslavcev@yandex.ru

<sup>5</sup> Shubnikov Institute of Crystallography, FSRC "Crystallography and Photonics" RAS, 119333 Moscow, Russia; natalya.arkharova@yandex.ru (N.A.); vvo@ns.crys.ras.ru (V.V.); eleonora.shtykova@gmail.com (E.S.)

\* Correspondence: tsne\_77@list.ru

**Abstract:** The search for materials for a new generation of wound coatings is important due to the increase in antibiotic-resistant microorganisms and the number of patients with untreatable chronic purulent wounds. Metal nanoparticles, specifically silver nanoparticles, have antimicrobial activity and do not induce known bacterial resistance. To obtain new Ag-containing nanocomposites, type I collagen was extracted by an enzyme–acid method from cattle tendons. Silver nanoparticles were obtained by an environmentally safe method, metal-vapor synthesis (MVS), which enables obtaining metal nanoparticles without impurities. For this, metal vapors were cocondensed in a vacuum of  $10^{-2}$  Pa on the walls of a quartz reactor cooled to 77 K using acetone as an organic dispersion medium. The composition of the collagen surface was determined by XPS using the spectra of C1s, N1s, and O1s. The presence of a peak with a binding energy of approximately 368.57 eV in the Ag 3d<sub>5/2</sub> spectrum indicates the state of Ag<sup>0</sup> silver atoms in the nanocomposite. SEM images showed that collagen contributes to the effective stabilization of Ag nanoparticles with an average size of  $13.0 \pm 3.5$  nm. It was found that collagen is non-toxic and biocompatible with skin cells and fibroblasts. The collagen–Ag nanoparticle nanocomposites exhibited antimicrobial activity against bacteria *Bacillus subtilis*, *Escherichia coli*, and fungi *Aspergillus niger*.

**Keywords:** wound coatings; collagen; silver nanoparticles; metal-vapor synthesis; antimicrobial activity



**Citation:** Vasil'kov, A.; Tseomashko, N.; Tretyakova, A.; Abidova, A.; Butenko, I.; Pereyaslvtsev, A.; Arkharova, N.; Volkov, V.; Shtykova, E. Wound Coating Collagen-Based Composites with Ag Nanoparticles: Synthesis, Structure and Biological Activity. *Coatings* **2023**, *13*, 1315. <https://doi.org/10.3390/coatings13081315>

Academic Editor: Giuseppe Cirillo

Received: 30 June 2023

Revised: 18 July 2023

Accepted: 24 July 2023

Published: 27 July 2023



**Copyright:** © 2023 by the authors. Licensee MDPI, Basel, Switzerland. This article is an open access article distributed under the terms and conditions of the Creative Commons Attribution (CC BY) license (<https://creativecommons.org/licenses/by/4.0/>).

## 1. Introduction

Wound coatings/dressings should be biodegradable, biocompatible, non-toxic, non-pyrogenic, non-allergenic, have good absorbency, adhesion, permeability to gases, water vapor, and, most importantly, have antimicrobial and regenerating activity [1]. Currently, there are no wound coatings that meet all the above requirements and this area is open for research. Based on the requirements of biodegradability and biocompatibility, collagen (Col) is the most suitable dressing material [2]. The use of biodegradable polymers makes it possible to solve environmental problems while creating a sustainable ecosystem [3]. Collagen has a highly ordered structure, chemical and thermal stability. It combines the positive qualities of synthetic polymers and does not have their negative sides [4]. Collagen is non-toxic, has low antigenicity due to the absence of histocompatibility receptors, is resistant to tissue enzymes, and is able to stimulate regenerative processes, cell proliferation and migration [5]. Collagen for biomedical, pharmaceutical and food purposes is extracted from skins, tendons, ligaments of cattle, pigs, fish waste (skin, bones) [6,7], and

sea mollusks [8,9]. The purest collagen with good yield is obtained from the tendons of the tails of cattle. Tendons consist only of type I collagen [10].

The growth of resistance of microorganisms to antibiotics is one of the most important problems of modern clinical practice. Despite the pace of development of antimicrobials, mortality rates from tissue damage and wound infections are quite high. All this stimulates the search for new effective antimicrobial drugs and wound coatings that do not cause resistance of microorganisms [11].

Collagen is a suitable matrix for wound coatings, which can be enriched with antimicrobial, anti-inflammatory, antioxidant and other drugs, and thus make the wound coating multifunctional. Thus, researchers offer wound coatings and collagen hydrogels with various antibiotics [12,13], collagen complexes with biologically active components [14,15], collagen complexes with hydroxyapatites and polysaccharides or lanthanum oxide or silicon dioxide for bone tissue regeneration, complexes with beta-tricalcium phosphate and strontium oxide for bone engineering [16–19]. Enrichment of the collagen matrix with polyphenolic compounds leads to collagen structuring and imparts additional properties to the material, such as antioxidant, anti-inflammatory, proliferative, and even antimicrobial properties [20,21]. Wound coatings with polyphenolic compounds—quercetin and rutin—accelerated the healing of experimental purulent wounds by 1.73 fold [21,22]. Hybrid complexes of collagen with metal nanoparticles are promising, since nanoparticles of many metals (silver, zinc, gold, titanium, etc.) have high antimicrobial activity in the absence of microbial resistance to them [1,23].

Nanosilver is currently used in wound coatings, cosmetic lotions, dental materials, antimicrobial textiles, wastewater treatment, etc. [24]. A significant antimicrobial effect of silver nanoparticles in the fight against various infections and diseases was demonstrated [25,26], as well as an effective wound coating based on hydrocollagen and silver nanoparticles in the treatment of purulent wounds [27]. The dose-dependent antimicrobial activity of collagen/ZnTiO<sub>3</sub> nanocomposites against Firmicutes (*Staphylococcus epidermidis*, *Bacillus cereus*), Gram-negative bacteria (*Escherichia coli*, *Salmonella enterica*, *Pseudomonas putida*) and fungi with low cytotoxicity on skin cell cultures has been previously demonstrated. The authors suggested three mechanisms of antimicrobial action: mechanical destruction of cell membranes by crystalline metal nanoparticles, its chelation with metal ions, and the formation of oxygen free radicals [28].

At the moment, there are many methods for the synthesis of metal nanoparticles of various compositions (pure metal, oxides, hydroxides, salts, etc.), size (1–100 nm) and shape (spherical, needles, plates, etc.). Methods for the reduction of metals using a wide range of reducing agents, such as sodium borohydride [29,30], trisodium citrate and glucose [20], tannic acid [31], triethanolamine [32], and ultraviolet radiation [33] have a number of significant limitations: a long synthesis process, the presence of a significant amount of impurities in the form of surfactants and residues of synthesis products, as well as the difficulty of controlling the completeness of metal reduction [34,35]. It should be noted that there are difficulties in controlling the formation of the internal structure of materials in the process of chemical reduction of metals, which arise due to the presence of impurities in the matrix. In recent years, biogenic or “green” synthesis of metal nanoparticles using bacteria, fungi, aquatic plants, and herbivorous animals has become popular [36]. The advantage of biogenic methods is that nanoparticles are regenerated from ions and stabilized by biomolecules produced by microorganisms that may be familiar to the human body. These methods also have similar limitations, which greatly complicate the use of the obtained materials for biomedical purposes [37–41]. Metal-vapor synthesis (MVS) has undoubted advantages, allowing the dispersion of metal components at the atomic level, significantly increasing the uniformity of their distribution [42]. This efficient environmentally friendly method for obtaining biologically active nanoparticles of metals and their oxides is widely used in the preparation of new biomedical hybrid metal polymers [43–46]. The MVS method is based on simultaneous processes of evaporation and condensation of metal and organic ligand on reactor walls cooled with liquid nitrogen under vacuum conditions of

$10^{-4}$ – $10^{-6}$  Torr. To date, nanoparticles of gold, silver, copper, nickel, cobalt, zinc, and many other metals have been obtained by the MVS method, “solvated” with various types of solvents [47–50]. The advantages of this method for obtaining metal nanoparticles include: the absence of synthesis by-products during the formation of metal nanoparticles; the possibility of obtaining nanoparticles of various metals, including those with pronounced antimicrobial activity and/or magnetic properties; the ease of modifying various types of supports, including polymer matrices, in order to impart new functional properties to them [48,51–53]. Nanocomposites based on natural polymers containing Ag nanoparticles (Ag NPs) obtained by MVS showed high antibacterial activity [54,55]. The fundamental possibility of using the MVS method to obtain medical supplies is shown in [56,57]. Unlike most methods for obtaining nanoparticles, MVS is an environmentally friendly closed cycle that can be effectively integrated into various technological processes for obtaining biologically active metal-containing composites.

Collagen and materials based on it are considered as the most promising biomaterials for clinical applications. The ease of modifying the surface of collagen with metal nanoparticles obtained by the MVS method makes it possible to improve its physicochemical and biological properties. In this work, for the first time, using the MVS method, biologically active Ag-containing nanocomposites based on collagen were obtained in the form of gels and porous materials—promising components for creating wound dressings.

## 2. Materials and Methods

Chemical reagents and media used in work: silver (purity 99.99%), acetone (Sigma-Aldrich, St. Louis, MO, USA, ACS reagent, purity  $\geq 99.5\%$ ), zeolites (4 Å), culture media RPMI-1640 (Himedia, Mumbai, India), fetal bovine serum FBS (Himedia, India),  $100\times$  antibiotic–antimycotic solution (Himedia, India), DMSO (Sigma, USA), EDTA (Sigma, USA), crystalline trypsin (SamsonMed, Saint Petersburg, Russia), 3-(4,5-dimethylthiazol-2-yl)-2,5-diphenyltetrazolium bromide MTT (Himedia, India), as well as chemicals reagents produced in the CIS countries. In the research, the following equipment and consumables were used: Mindray MR-96A immunoassay analyzer (Mindray, Shenzhen, China), Thermostat TS-1/80 SPU (JSC “Smolensk SKTB SPU”, Smolensk, Russia), water purification system “Prodion” 10VS-MA (JSC “Vital Development Corporation” Saint Petersburg, Russia), Tabletop centrifuge TDZ4-4WS (Changsha Weierkang Xiangying Centrifuge Co., Ltd., Changsha, China), BIOBASE  $-60\text{ }^{\circ}\text{C}$ – $-80\text{ }^{\circ}\text{C}$  vacuum lyophilizer freeze dryer machine BK-FD12PT (BIOBASE Group, Jinan, China),  $\text{CO}_2$ -Incubator (Shel Lab, Cornelius, OR, USA), Laminar flow cabinet BBS-V1800-XK (BIOBASE Group, Jinan, China), Bante210 Benchtop pH Meter (Bante Instruments Co., Ltd., Shanghai, China), Yx280b portable autoclave (WINCOM COMPANY LTD., Changsha, China), microscope Leica DM IL LED (Leica Microsystems Inc., Wetzlar, Germany), microscope Zeiss Axiolab A1 (Carl Zeiss AG, Oberkochen, Germany), digital video camera SDPTOP,  $50\text{ cm}^2$  culture flasks and Petri dishes (Costar, Washington, DC, USA), 24-well and 96-well plates (Costar, Washington, DC, USA).

### 2.1. Obtaining Collagen from Biological Raw Materials

Powdered collagen was obtained from cow tail tendons using both enzymatic and acid extraction methods [58]. Trypsin was used as an enzyme. The tendons of the tails of cows were cleaned from muscles, ligaments and skin, crushed to pieces 1–2 mm in size, treated with 0.25% trypsin solution at  $37\text{ }^{\circ}\text{C}$  for 3 h. The resulting suspension was diluted with distilled water at the rate of 1:100 and precipitated in a centrifuge at 3000 rpm for 10 min in order to remove non-collagen proteins. Next, the precipitate was subjected to hydrolysis in a 0.1 N solution of acetic acid (1:100) for 48 h. The collagen solution was then precipitated in a centrifuge at 3000 rpm for 10 min. The collagen precipitate was filtered through a mesh material to remove large pieces, which were re-hydrolyzed. The collagen was then dialyzed against water and lyophilized. To form porous materials, dialyzed collagen was poured into special flasks and frozen at  $-30\text{ }^{\circ}\text{C}$ . After that, the flasks were

placed in a chilled freeze-drying chamber for lyophilization (pressure in the apparatus 13.3322–66.6610 N/m<sup>2</sup>). Lyophilization lasted an average of 17 h at a working temperature of −70 °C.

### 2.2. Modification of Collagen by Silver Nanoparticles Obtained by Metal-Vapor Synthesis

MVS was carried out by co-condensation of vapors of metal and organic reagents in a vacuum of 10<sup>−2</sup> Pa on the walls of a 5 L quartz reactor cooled to −196 °C. The metal was evaporated by resistive heating from a tantalum evaporator. The organic solvent acetone was dried over zeolites and degassed by alternating freeze–thaw cycles. After the completion of metal evaporation, the supply of the organic reagent was stopped. The cooling was removed, the co-condensate was heated until melting. After the matrix was defrosted, the organosol was removed from the reactor through a siphon system into a prepared evacuated flask containing dialyzed collagen gel in water. During in situ application, the mixture was stirred with a magnetic stirrer and the flask was filled with argon. Next, the flask was disconnected from the siphon line and the resulting mixtures were stirred for 60 min. At the end of the deposition process, the metal-containing matrix was decanted from the organic solvent and dried in a vacuum (10<sup>−1</sup> Pa) at 60 °C to constant weight. After distillation in vacuo from the solvent gel, the residue was freeze-dried.

### 2.3. Obtaining Fibroblast Cell Cultures to Assess the Cytotoxicity and Biocompatibility of Collagen

Fibroblasts were obtained using the explant method proposed in [21]. Cells were cultured in complete growth medium RPMI-1640 (Himedia, India) containing 10% FBS (Himedia, India) and 1% antibiotic–antimycotic solution (Himedia, India, where 10,000 U/mL penicillin, 10,000 µg/mL streptomycin and 25 µg/mL amphotericin B) in a CO<sub>2</sub> incubator (ShelLab, Cornelius, OR, USA) at +37 °C, 5% CO<sub>2</sub>. The medium was changed every 4 days. When the cell culture reached 80% confluency, the cells were reseeded (multiplicity of sieving 1:3). For studies, stabilized cell cultures were used after 5 passages.

### 2.4. Determination of the Number of Living Cells on a Collagen Substrate by Staining with a Vital Dye in the MTT Assay

Under sterile conditions, 10 mL of collagen gel was poured into 24-well plates and the plates were left open for collagen polymerization in nitrogen vapor and under ultraviolet radiation for 10 min. A commercial preparation of collagen film NeuSkin-F (Eucare Pharmaceuticals (P) Limited, India) was used as a reference. To do this, circles with a diameter of 15 mm were cut out from NeuSkin-F films and placed in the wells of 24-well plates. Stabilized fibroblast cells were removed from the bottom of culture flasks with a trypsin-EDTA solution. The number of cells was counted and diluted with complete growth medium RPMI-1640. Fibroblast cells were seeded on collagen substrates in 24-well plates at the rate of 1 × 10<sup>4</sup> cells per well in 1 mL of complete medium and the plates were left for 24, 48 and 72 h in a CO<sub>2</sub> incubator.

After 24, 48 and 72 h, the medium was removed from the wells and 0.8 mL of incomplete medium, without FBS and antimycotic-antibiotic, and 0.2 mL of the MTT solution were added to each well, having previously dissolved 5 mg of MTT (SIGMA, St. Louis, MO, USA) in 1 mL sterile PBS solution (pH 7.2) and filtered. The plates were protected from light and incubated at 37 °C for 4 h. After the incubation period, the wells were emptied and 1 mL of the organic solvent dimethyl sulfoxide, DMSO (SIGMA, USA), was added to each well. After 10 min, readings were taken on a microplate spectrophotometer (Mindray MR-96A, China) at a wavelength of 596 nm.

Cell survival in the presence of the test samples was calculated by the formula: (OD of experimental wells – OD of medium)/(OD of control wells – OD of medium) × 100%, where OD is the optical density. Intact cells served as controls.

All data were presented as the mean ± standard deviation of three independent triplicate experiments (3 plates × 3 wells per sample). The data were statistically processed

using Student's paired *t*-test. Mean values were considered statistically significant at  $p < 0.05$ .

#### 2.5. Scanning Electron Microscopy (SEM)

The morphology of the surface of the original and modified collagen matrixes was studied by low-voltage scanning electron microscopy (LVSEM) on an FEI Scios microscope (Thermo Fisher Scientific, Waltham, MA, USA) in the secondary and backscattered electron mode with an accelerating voltage of less than 1 kV.

#### 2.6. Thermogravimetric Analysis (TGA)

Thermogravimetric analysis was carried out using a Derivatograph-C device (MOM, Mátészalka, Hungary) device at a heating rate of 10 °C/min in air up to 650 °C.

#### 2.7. Powder X-ray Diffraction (PXRD)

Powder X-ray diffraction phase analysis was performed with a D8 Advance (Bruker AXS, Karlsruhe, Germany) diffractometer in Bragg–Brentano focusing geometry using  $\text{CuK}\alpha$  radiation and an angular range of 5–90° with a step of 0.02° and scan rate of 0.5–2 deg/min. The samples were placed on flat holders. Diffraction pattern profiles were fit using the TOPAS 5 program package (Bruker AXS, Karlsruhe, Germany).

#### 2.8. Small-Angle X-ray Scattering (SAXS)

SAXS measurements were performed on a laboratory diffractometer (AMUR-K, Institute of Crystallography, Moscow, Russia) at a wavelength  $\lambda = 0.1542$  nm in a Kratky-type (infinitely long slit) geometry covered the range of momentum transfer  $0.12 < s < 7.0$  nm<sup>-1</sup> (here,  $s = 4\pi \sin\theta/\lambda$ , where  $2\theta$  is the scattering angle). The scattering profiles were corrected for the background scattering and primarily processed using the program PRIMUS [59] of the software suit ATSAS [60]. The experimental SAXS data were normalized for the intensity of the incident beam, and then a correction for the collimation distortion was made in accordance with the standard procedure [61].

The processed experimental SAXS curves were used to compute the volume size distribution functions  $D_V(R)$  of the scattering particles. Assuming the particles to be spherical, an indirect transform program GNOM [62] was employed to solve the integral equation.

#### 2.9. X-ray Photoelectron Spectroscopy (XPS)

The XPS analysis was performed using a Thermo Fisher Scientific Theta Probe spectrometer (ThermoFisher Scientific Ltd., East Grinstead, UK). For analysis, a monochromatic Al  $\text{K}\alpha$  (1486.6 eV) X-ray source was used. The spectra were measured at room temperature at a pressure of  $\sim 5 \times 10^{-10}$  mbar in the analytical chamber. The energy scale of the spectrometer was calibrated to provide the following values for reference samples: Au 4f<sub>7/2</sub>–83.96 eV, Cu 2p<sub>3/2</sub>–932.62 eV, Ag 3d<sub>5/2</sub>–368.21 eV. Survey spectra were recorded at constant pass energies of 300 eV, with step sizes of 1 eV, delay time 0.05 s, number of scans 5. High-resolution spectra of appropriate core levels were recorded at constant pass energies of 100 eV, with step sizes of 0.1 eV, delay time 0.1 s, number of scans 15 [63]. The samples were mounted on a titanium sample holder with two-sided adhesive tape.

In the process of recording the spectra, the differential charging of the sample was compensated using a low-energy electron beam. The charge of the sample was corrected by reference to the C-C/C-H state identified in the C 1s spectrum (285.0 eV). After binding to the charge, the Shirley-type background was subtracted from the high-resolution spectra and the approximation by the Gaussian function or the sum of the Gaussian functions was carried out. Quantitative analysis was carried out using the survey spectrum and elemental sensitivity coefficients included in the software of the spectrometer.

### 2.10. Antimicrobial Tests

The antimicrobial activity of the composites was measured by the disk diffusion method. A sample of Ag—containing collagen 6 × 6 mm in size was used. The spectrum of antibacterial activity was studied using test cultures of strains of Gram-positive bacteria—*Bacillus subtilis* ATCC 6633 and Gram-negative bacteria—*Escherichia coli* ATCC 25922. Antifungal activity was assessed using the *Aspergillus test strain. Niger* INA 760 from the collection of cultures of the Institute of New Antibiotics, Gauze (Moscow, Russia). Bacteria and fungi were incubated at 37 °C within 24 h. Standard disks with antibiotics were used as positive controls (ampicillin—10 µg/disk, amphotericin B—40 µg/disk, produced by the Pasteur Institute (St. Petersburg, Russia)).

### 3. Results and Discussion

New materials based on collagen modified with nanoparticles of biologically active metals may be promising for creating wound dressings. This is due to the fact that collagen has a high biocompatibility and the ability to stimulate the growth and division of connective tissue cells [64], and the introduction of silver nanoparticles imparts antibacterial properties to the hybrid material.

The yield of the collagen obtained only from the tendons of the tail of cattle by the method mentioned in Section 2.1 was 2.24%. However, in [64] the yield of the target product from by-products of sheep slaughter was 12.5%–18.0% in terms of dry matter. The collagen prepared in [65] cannot be of the same type, since the authors isolated collagen from bones, skin, and tendons. This raw material contains, in addition to type I collagen, collagens of other types that are not suitable for biomedical purposes. Collagen extracted from tendons consists mainly of type I collagen and is more suitable for biomedical applications.

The assessment of the biocompatibility of the prepared collagen was carried out by the in vitro method, by seeding secondary cultures of fibroblast cells on substrates from this collagen. NeuSkin-F commercial collagen film (India) was used as a comparison drug (reference drug). After 24, 48 and 72 h of incubation of fibroblast cells on substrates from the obtained collagen and NeuSkin-F, fibroblast viability was assessed using the vital dye MTT. Cells seeded in the wells of the plate without substrate served as a control and were taken as 100% live cells. The experiment was set in 9 repetitions (3 plates × 3 wells per sample) and the average value was derived (Table 1). As a result of the study, it was found that the collagen preparation we received and NeuSkin-F comparisons are not cytotoxic and biocompatible with fibroblasts. A slight proliferative activity of fibroblasts was observed during prolonged (72 h) incubation of cells on the substrates under study. This shows that collagen and NeuSkin-F are better substrates for fibroblast adhesion and growth than culture plate surfaces.

**Table 1.** Evaluation of the biocompatibility of collagen and fibroblast cells.

Sample	Number of Living Cells, %		
	24 h	48 h	72 h
Col	97.6 ± 0.3	106.2 ± 0.5	110.5 ± 0.4
NeuSkin-F	98.3 ± 0.2	108.1 ± 0.3	119.0 ± 0.6

For the first time, hybrid materials based on a biocompatible polymer matrix—collagen—and Ag nanoparticles obtained by the MVS method using acetone as a dispersion medium were prepared. The composition, structure and electronic state of the metal in the materials were characterized by modern physicochemical methods.

SEM images of the surface morphology of the initial and modified collagen are shown in Figures 1 and 2. Previously, this technique was used to study catalytically active systems based on chitosan [66]. The wide collagen strands, including fibers up to 100 nm in size, and forming a network of interpenetrating pores in a wide range from hundreds of nanometers to approximately 20–30 µm, present the natural structure of initial collagen

matrix. Modifying collagen matrix by silver nanoparticles synthesized by the MVS method does not change the collagen microstructure: the strands and the individual fibers of collagen are clearly visualized in the SEM image obtained in the secondary electron (SE) mode (Figure 2a). In the same image obtained in the backscattered electron (BSE) mode Ag NPs can be detected as the silver shows brighter contrast due to the higher molar weight (Figure 2b). The even contrast in the BSE image indicates a uniform distribution of silver nanoparticles on the surface of collagen, with the exception of small rare clusters up to 100 nm. SEM image of the individual fiber confirms the uniform distribution of Ag NPs through the fiber (Figure 2b, inset). To estimate the size range of the Ag particles through the collagen fibers several independent fibers with near 1000 particles on average were taken into the account. Thus, the Ag NPs size varies from several nanometers to 35 nm with an average size of  $13.0 \pm 3.5$  nm.

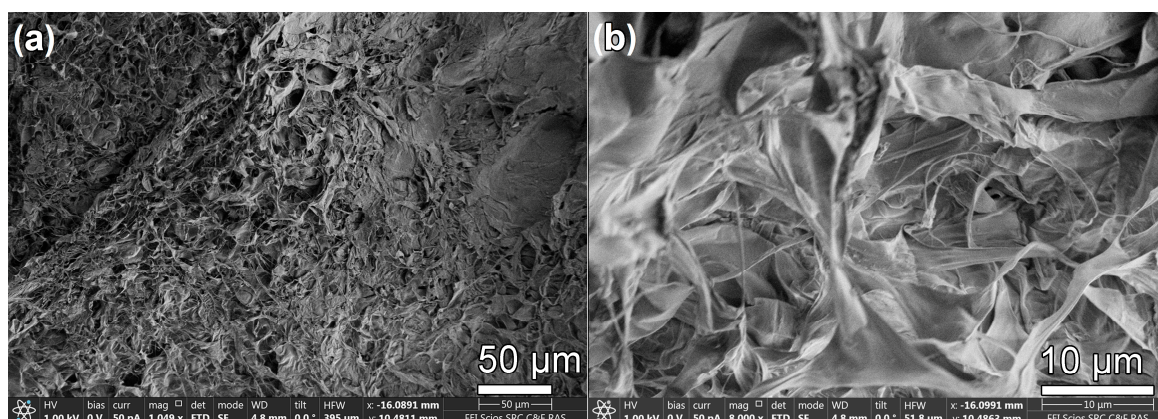


**Figure 1.** SEM images of the surface morphology of the initial collagen matrix with different magnifications: (a) 50  $\mu$ m; (b) 10  $\mu$ m.

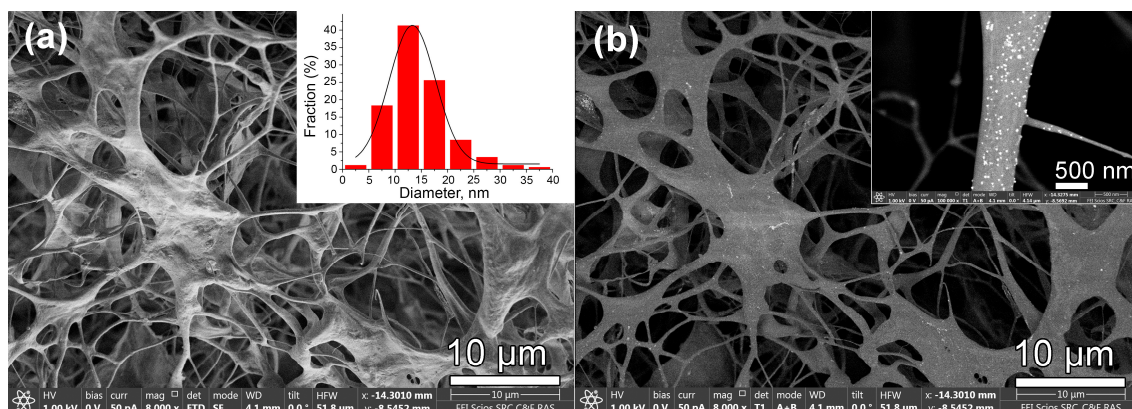


**Figure 2.** SEM images of the surface of modified collagen with silver nanoparticles Col/Ag NPs: (a) in the SE mode; (b) in the BSE mode. An individual collagen fiber with silver nanoparticles on it with corresponding histogram of NPs size distribution is presented as an inset.

Thermal behavior of the nanocomposite Col/Ag NPs was studied by thermogravimetric analysis.

The weight loss of the studied samples in air proceeds in several stages (Figure 3). At the first, ending in the region of 100 °C, the moisture sorbed from the air is removed. The main processes of collagen decomposition proceed in the range of 250–400 °C; with a further increase in temperature, the destructive processes slow down and continue at a much lower rate, up to 700 °C [67].

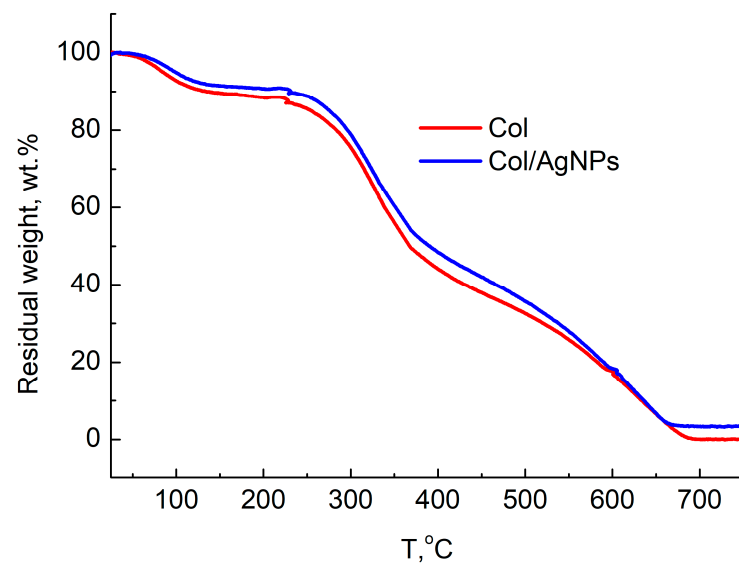


**Figure 3.** Thermogravimetric curves of Col (red) and Col/Ag NPs (blue).

A comparative analysis of the TGA parameters of pure collagen and Ag-containing composite showed that the modification of collagen with metal nanoparticles has little effect on the process of its thermal degradation.

The nanocomposites Col/Ag NPs were studied by the powder X-ray diffraction method. The absence of pronounced reflexes in the diffractogram of collagen indicates its amorphous nature. In this regard, all the observed peaks can be characteristic of the fcc packing of metal nanoparticles (Figure 4). Peaks are observed at  $2\theta$  angles of  $38.1^\circ$  (111),  $44.3^\circ$  (002),  $64.5^\circ$  (022),  $77.4^\circ$  (311) and  $81.5^\circ$  (222). In the sample under consideration, the silver phase is uniquely identified. Estimated by the Scherrer formula size metal nanoparticles in the composition of composite materials Col/Ag NPs was 23 nm.

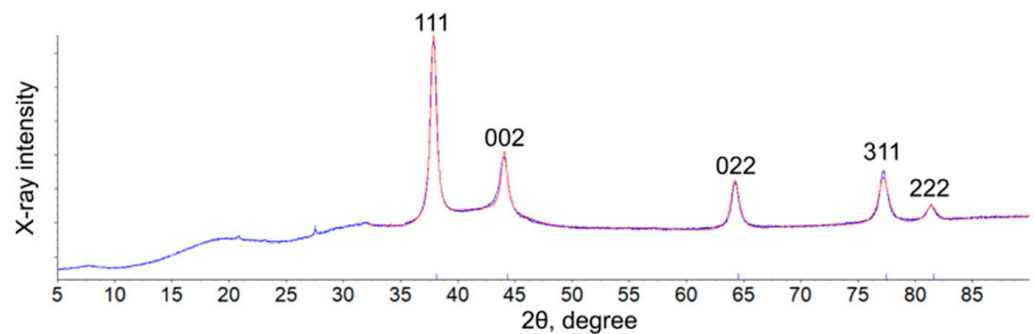


**Figure 4.** PXRD pattern of the Col/Ag NPs composite (blue line) and its fit evidencing the presence of Ag nanoparticles (red line).

Small-angle X-ray scattering was applied to study Col and Col/Ag NPs. The corresponding scattering curves are shown in Figure 5a.

Experimental SAXS curves from Col and Col/Ag NPs were collected in the range of momentum transfer  $0.12 < s < 7.0 \text{ nm}^{-1}$ ; however, due to strong experimental noise at  $s > 2 \text{ nm}^{-1}$ , the region only up to  $2 \text{ nm}^{-1}$  was used for further analysis. As one can see from Figure 5a pure collagen Col exhibits the low scattering even at very small angles, which is characteristic of a nearly homogeneous medium. In such samples, there are practically no structural inhomogeneities (pores or compactions) and, therefore, the calculation of size distributions is meaningless in this case. The incorporation of the Ag nanoparticles into collagen gels leads to a significant increase in the scattering intensity due to the higher electron density of the metal compared to the gel.

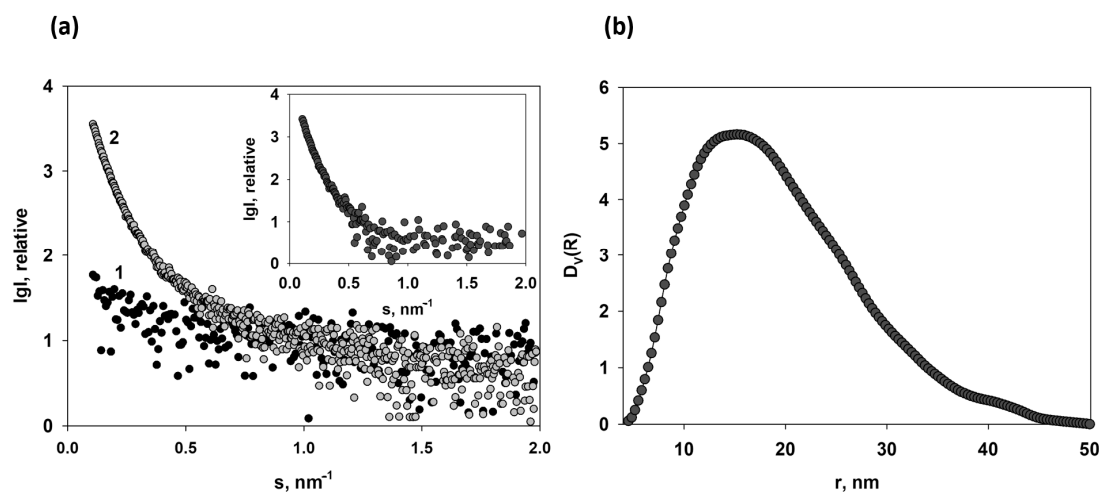


**Figure 5.** (a): Experimental SAXS curves from Col (curve 1) and Col/Ag NPs (curve 2). Inset: the difference scattering curve obtained by subtracting the Col scattering from that of Col/Ag NPs. (b): The volume size distribution functions  $D_V(R)$  calculated from the difference scattering curve shown in the inset of the panel (a).

Despite the fact that the intensity of the scattering from the gel with the embedded metal nanoparticles is much higher than the scattering from the initial gel and, thus, the scattering from the latter could be neglected, for a more accurate determination of the size distribution of the Ag nanoparticles, the scattering from the gel should be subtracted from the total scattering. In this way, scattering from the metal nanoparticles only will be calculated. The obtained difference scattering profile is shown in the inset of Figure 5a. This curve was used for calculation of the volume size distribution function  $D_V(R)$  of Ag nanoparticles embedded in the Col (Figure 5b).

The gel-stabilized Ag nanoparticles exhibit a relatively broad monomodal size distribution with radii up to 50 nm and the most popular radii being approximately 14–16 nm. It should be noted that the fraction of the metal particles larger than 30 nm is relatively small. Hence, we can conclude that the stabilization of the Ag nanoparticles by the Col is quite effective.

The interaction of Ag NPs with the collagen surface can change the electronic structure of both the metal and the material as a whole. Photoelectron spectroscopy is the leading method for analyzing various physicochemical characteristics of nanostructured elements on the metal surface.

Analysis of the survey spectra (Figure 6) allowed estimation of the relative concentrations of elements on the surface of Col and Col/Ag NPs samples. The results are presented in Table 2.

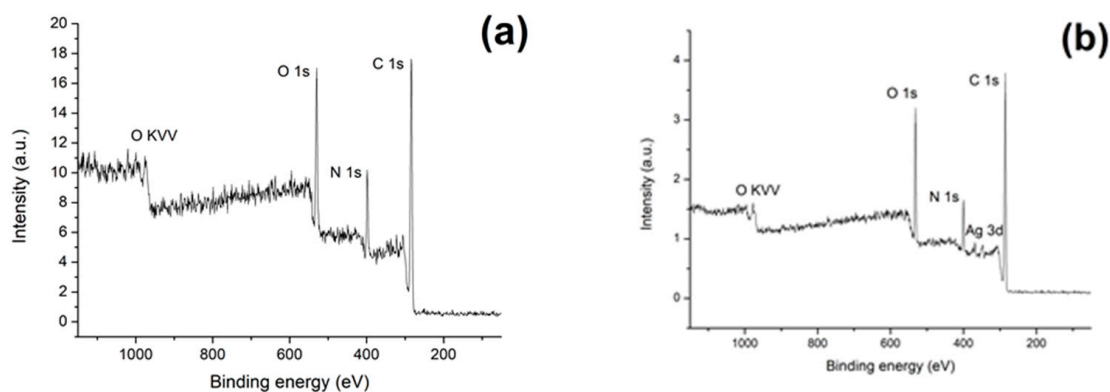
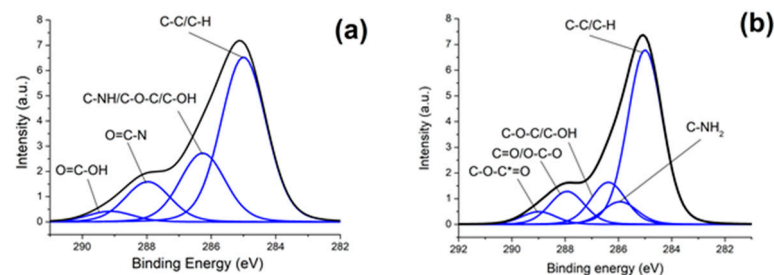


**Figure 6.** Full XPS spectrum of the samples Col (a) and Col/Ag NPs (b).

**Table 2.** Concentrations of elements on the surface of Col and Col/Ag NPs samples (at. %), calculated from the XPS spectra.

Sample	C	N	O	Ag
Col	52	15	32	–
Col/Ag NPs	74	9	17	0.1

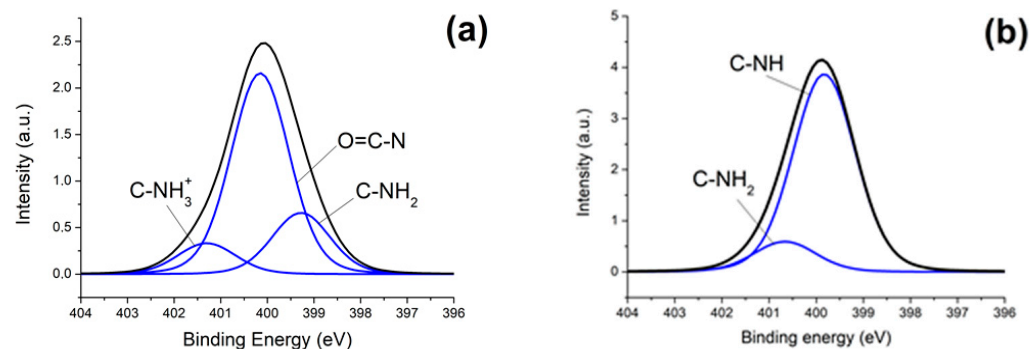
Collagen is a repeating sequence of Gly-Pro-Hyp amino acids [68]. According to this, the model C 1s spectrum of collagen should contain the states C-C/C-H, C-N-H, C-OH, O-C=O, N-C=O [63]. The characteristics of the four states are usually used to describe such systems [69,70]. This is due to the fact that the range of chemical shifts of the C-N-H, C-O-C, C-OH, and O-C=O bonds overlaps to a large extent [63] and can be replaced by the total peak, simplifying the model [70,71]. The chemical shift of the C=O/O-C-O/N-C=O bonds is within 0.2 eV with respect to each other, which in the case of massive non-conductive samples leads to overlapping or merging of the peaks due to the presence of differential charging, which cannot be fully compensated. Figure 7 presents the C 1s Col and Col/Ag NPs spectra as the sum of several Gaussian profiles using the reference chemical shifts for the respective chemical groups [63]. Table S1 (see Supplementary Materials) presents the characteristics of the peaks.



**Figure 7.** The C 1s photoelectron spectrum of Col (a) and Col/Ag NPs (b). The black line is the sum of all Gaussian components.

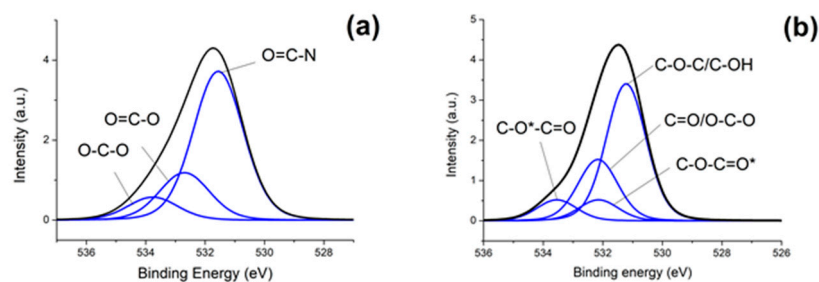
Comparative analysis of C 1s spectrum showed that the surface composition of Col and Col/Ag NPs significantly differs. This may be caused by a change in the chemical composition of the collagen surface after its modification with Ag NPs/acetone organosol.

Figure 8 shows the N 1s spectrum of Col and Col/Ag NPs samples, and Table S1 shows peak characteristics. The typical N 1s spectrum of collagen in the literature is described by the three principal states C-NH<sub>2</sub>, N-C=O, and C-NH<sub>3</sub><sup>+</sup>, whose binding energies are 399.6, 400.5 and 401 eV, respectively [63,72]. It should be noted that the content of the amide groups decreased, which, as well as the changes in the C 1s spectrum, may indicate damage to the peptide chain.



**Figure 8.** The N 1s photoelectron spectrum of Col (a) and Col/Ag NPs (b). The black line is the sum of all Gaussian components.

In Figure 9a, the O-C=O group is the sum of two peaks of equal intensity C-O\*-C=O and C-O-C=O\* with a small difference in energy values (less than 1.38 eV), which can be replaced by a single total peak if the differential charge is negligible [63]. This may be a sign of the “balancing” of the two oxygen species and the formation of the tertiary structure of the protein. For the sample with silver, there seems to be a decrease in the differential charge. This is manifested by a narrowing of the peaks and an increase in the energy difference between the peaks of the O-C=O grouping to typical values of 1.4 eV, which makes it possible to fit/leave both peaks in the spectrum decomposition instead of using the summed peak. Analysis of the data presented in Figure 9b suggests that modification of collagen by silver nanoparticles disrupts the protein structure.



**Figure 9.** The O 1s photoelectron spectrum of Col (a) and Col/Ag NPs (b). The black line is the sum of all Gaussian components. The label \* indicates the state of a particular oxygen atom.

Parameters of the C 1s, N 1s and O 1s spectrum are presented in Table S1.

Figure 10 shows the spectrum of the Ag 3d nanocomposite Col/Ag NPs, and Table 3 shows the characteristics of the peaks. The spectrum of the Ag 3d sample registers a characteristic doublet with a spin splitting of 6 eV. For the Ag 3d<sub>5/2</sub> peak, silver Ag, Ag<sub>2</sub>O, and AgO states with average binding energies of 368.2, 367.8, and 367.4 eV, respectively, are reported in the literature [63,68,73–77]. The low concentration of Ag makes it difficult to determine the chemical state of the metal using the modified Auger parameter. Analysis of the results obtained allows us to attribute a binding energy of 368.57 eV to the metallic state of silver. The difference between the binding energy of the Ag 3d<sub>5/2</sub> peak of the reference sample used in the spectrometer calibration and the Col/Ag NPs sample can be due to the dimensional effect due to the nanometer parameters of silver particles.

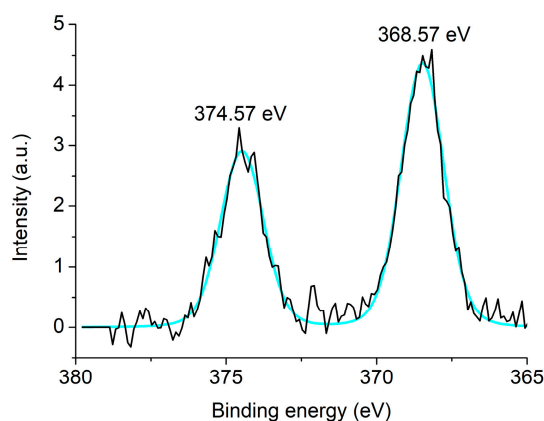


**Figure 10.** The Ag 3d photoelectron spectrum of Col/Ag NPs.

**Table 3.** Characteristics of photoelectron spectrum for Col/Ag NPs: binding energies ( $E_b$ ), spin–orbit splitting (SOS), and state.

Sample	$E_b$ Ag 3d <sub>5/2</sub> , eV	$E_b$ Ag 3d <sub>3/2</sub> , eV	SOS, eV	State
Col/Ag NPs	368.57	374.57	6.0	Ag <sup>0</sup>

Antimicrobial activity of freeze-dried nanocomposite Col/Ag NPs were determined by the disk diffusion method. The spectrum of antibacterial activity was studied using test cultures of strains of Gram-positive and Gram-negative bacteria, and antifungal activity was also tested. Standard disks with antibiotics were used as controls (Figure S1, see Supplementary Materials). The results are presented in Table 4.

**Table 4.** Antimicrobial activity of Col/Ag NPs.

Sample	Zone of Inhibition, mm		
	<i>B. subtilis</i> TCC 6633	<i>E. coli</i> ATCC 25922	<i>A. niger</i> INA 00760
Col/Ag NPs	6.5 ± 0.4	11.3 ± 0.7	6.5 ± 0.4
ampicillin	30.7 ± 1.0	27.0 ± 1.7	* nt
amphotericin B	* nt	* nt	15.3 ± 0.3

\* nt—non-tested.

Table 4 shows the hybrid material Col/Ag NPs inhibits the growth of the present fungal and bacterial cells, but is weaker than the antifungal amphotericin B and the antibiotic ampicillin. Nevertheless, the effect of the obtained new Col/Ag NPs in further studies will need to be tested on experimental purulent wounds, especially on wounds contaminated with antibiotic-resistant microorganisms.

#### 4. Conclusions

New hybrid materials with antibacterial activity, based on collagen, modified with a silver-containing organosol were obtained using metal-vapor synthesis. SEM images showed that collagen contributes to the effective stabilization of Ag nanoparticles with an average size of  $13.0 \pm 3.5$  nm. A comparative analysis of the TGA parameters of pure collagen and Ag-containing composite showed that the modification of collagen with metal nanoparticles has little effect on the process of its thermal degradation. XPS results showed that the collagen/Ag NPs composite contained Ag<sup>0</sup> states. Collagen-based nanocomposite with Ag nanoparticles exhibited antimicrobial activity against *Bacillus subtilis*, *Escherichia coli* bacteria and *Aspergillus niger* fungi. The obtained material can be recommended for further research as a wound coating for the treatment of purulent wounds, fungal infections, etc.

The main difference in the prepared hybrid material is that the Col/Ag NP was obtained on the basis of type I collagen, which is the most suitable for medical purposes, and silver nanoparticles synthesized by the MVS method. MVS is a “green chemistry” method and makes it possible to obtain metal nanoparticles without impurities and by-products, which is also important for obtaining materials for biomedical purposes.

The new approach to the synthesis of hybrid metal–polymer systems presented in the work can make a significant contribution to the creation of a new generation of wound coatings.

**Supplementary Materials:** The following supporting information can be downloaded at: <https://www.mdpi.com/article/10.3390/coatings13081315/s1>, Figure S1: Antimicrobial activity of nanocomposite Col/Ag NPs. a: *B. subtilis*, 1—Col/Ag NPs and 2—ampicillin; b: *E. coli*, 1—Col/Ag NPs and 2—ampicillin; c: *A. niger*, 1—Col/Ag NPs and 2—amphotericin B. Table S1: Parameters of components in the photoelectron spectra of the collagen and its nanocomposite with silver nanoparticles: E<sub>b</sub>—binding energy, W—peak width and I<sub>rel</sub>—relative intensity.

**Author Contributions:** Conceptualization, supervision, nanomaterials synthesis, and writing—review and editing, A.V.; synthesis of collagen, investigation, and writing—review and editing, N.T.; project administration, nanomaterial synthesis, and writing—original draft preparation, A.T.; synthesis of collagen, investigation, and writing—original draft preparation, A.A.; biology methodology and nanoparticles synthesis, I.B.; investigation and material characterizations, A.P.; investigation, material characterizations, and formal analysis, N.A.; investigation and material characterizations, V.V.; material characterizations and writing—original draft preparation, E.S. All authors have read and agreed to the published version of the manuscript.

**Funding:** This research received no external funding.

**Institutional Review Board Statement:** Not applicable.

**Informed Consent Statement:** Not applicable.

**Data Availability Statement:** Not applicable.

**Acknowledgments:** This work was supported by the Ministry of Science and Higher Education of the Russian Federation (Contract No. 075-03-2023-642) and was performed employing the equipment of Center for molecular composition studies of INEOS RAS and within the State assignment of Federal Scientific Research Center “Crystallography and Photonics” of Russian Academy of Sciences in part of SAXS measurements and data interpretation and in part of electron microscopy study.

**Conflicts of Interest:** The authors declare no conflict of interest.

## References

1. Sabarees, G.; Velmurugan, V.; Tamilarasi, G.P.; Alagarsamy, V.; Solomon, V.R. Recent Advances in Silver Nanoparticles Containing Nanofibers for Chronic Wound Management. *Polymers* **2022**, *14*, 3994. [[CrossRef](#)]
2. Norouzi, M.; Boroujeni, S.M.; Omidvarkordshouli, N.; Soleimani, M. Advances in Skin Regeneration: Application of Electrospun Scaffolds. *Adv. Healthc. Mater.* **2015**, *4*, 1114–1133. [[CrossRef](#)] [[PubMed](#)]
3. Chang, H.; Feng, H.; Wang, R.; Zhang, X.; Wang, J.; Li, C.; Zhang, Y.; Li, L.; Ho, S.-H. Enhanced energy recovery from landfill leachate by linking light and dark bio-reactions: Underlying synergistic effects of dual microalgal interaction. *Water Res.* **2023**, *231*, 119578. [[CrossRef](#)] [[PubMed](#)]
4. Pallaske, F.; Pallaske, A.; Herklotz, K.; Boese-Landgraf, J. The significance of collagen dressings in wound management: A review. *J. Wound Care* **2018**, *27*, 692–702. [[CrossRef](#)] [[PubMed](#)]
5. Kempf, M.; Miyamura, Y.; Liu, P.Y.; Chen, A.C.H.; Nakamura, H.; Shimizu, H.; Tabata, Y.; Kimble, R.M.; McMillan, J.R. A denatured collagen microfiber scaffold seeded with human fibroblasts and keratinocytes for skin grafting. *Biomaterials* **2011**, *32*, 4782–4792. [[CrossRef](#)] [[PubMed](#)]
6. Fuente, D.; Tornos, A.; Princep, A.; Lorenzo, J.M.; Pateiro, M.; Berrada, H.; Barba, F.J.; Ruiz, M.-J.; Martí-Quijal, F.J. Scaling-up Processes: Patents and Commercial. *Adv. Food Nutr. Res.* **2020**, *92*, 187–223. [[CrossRef](#)]
7. Shelah, O.; Wertheimer, S.; Haj-Ali, R.; Lesman, A. Coral-derived Collagen Fibers for Engineering Aligned Tissues. *Tissue Eng. Part A* **2021**, *27*, 187–200. [[CrossRef](#)]
8. Claverie, M.; McReynolds, C.; Petitpas, A.; Thomas, M.; Fernandes, S.C.M. Marine-Derived Polymeric Materials and Biomimetics: An Overview. *Polymers* **2020**, *12*, 1002. [[CrossRef](#)]
9. Nurilmala, M.; Hizbullah, H.H.; Karnia, E.; Kusumaningtyas, E.; Ochiai, Y. Characterization and Antioxidant Activity of Collagen, Gelatin, and the Derived Peptides From Yellowfin Tuna. *Mar. Drugs* **2020**, *18*, 98. [[CrossRef](#)]
10. Maistrenko, L.; Iungin, O.; Pikus, P.; Pokholenko, I.; Gorbatiuk, O.; Moshynets, O.; Okhmat, O.; Kolesnyk, T.; Potters, G.; Mokrousova, O. Collagen Obtained from Leather Production Waste Provides Suitable Gels for Biomedical Applications. *Polymers* **2022**, *14*, 4749. [[CrossRef](#)]
11. Zille, A.; Fernandes, M.M.; Francesko, A.; Tzanov, T.; Fernandes, M.; Oliveira, F.R.; Almeida, L.; Amorim, T.; Carneiro, N.; Esteves, M.F.; et al. Size and aging effects on antimicrobial efficiency of silver nanoparticles coated on polyamide fabrics activated by atmospheric DBD plasma. *ACS Appl. Mater. Interfaces* **2015**, *7*, 13731–13744. [[CrossRef](#)] [[PubMed](#)]
12. Van Vugt, T.A.G.; Walraven, J.M.B.; Geurts, J.A.P.; Arts, J.J.C. Antibiotic-Loaded Collagen Sponges in Clinical Treatment of Chronic Osteomyelitis: A Systematic Review. *J. Bone Jt. Surg. Am.* **2018**, *100*, 2153–2161. [[CrossRef](#)] [[PubMed](#)]
13. Yıldırım, M.A.; Çakır, M.; Fındık, S.; Kişi, Ö.; Şentürk, M. Comparison of the efficacy of growth factor collagen and antibiotic collagen on colon anastomosis in experimental animals with peritonitis. *Indian J. Gastroenterol.* **2021**, *40*, 309–315. [[CrossRef](#)] [[PubMed](#)]
14. Berechet, M.D.; Gaidau, C.; Miletic, A.; Pilic, B.; Răpă, M.; Stanca, M.; Ditu, L.M.; Constantinescu, R.; Lazea-Stoyanova, A. Bioactive Properties of Nanofibres Based on Concentrated Collagen Hydrolysate Loaded with Thyme and Oregano Essential Oils. *Materials* **2020**, *13*, 1618. [[CrossRef](#)]
15. Ying, H.; Zhou, J.; Wang, M.; Su, D.; Ma, Q.; Lv, G.; Chen, J. In situ formed collagen-hyaluronic acid hydrogel as biomimetic dressing for promoting spontaneous wound healing. *Mater. Sci. Eng. C Mater. Biol. Appl.* **2019**, *101*, 487–498. [[CrossRef](#)]
16. Nogueira, L.F.B.; Cruz, M.A.E.; Aguilar, G.J.; Tapia-Blácido, D.R.; da Silva Ferreira, M.E.; Maniglia, B.C.; Bottini, M.; Ciancaglini, P.; Ramos, A.P. Synthesis of Antibacterial Hybrid Hydroxyapatite/Collagen/Polysaccharide Bioactive Membranes and Their Effect on Osteoblast Culture. *Int. J. Mol. Sci.* **2022**, *23*, 7277. [[CrossRef](#)]
17. Vijayan, V.; Sreekumar, S.; Ahina, K.M.; Lakra, R.; Kiran, M.S. Lanthanum Oxide Nanoparticles Reinforced Collagen  $\kappa$ -Carrageenan Hydroxyapatite Biocomposite as Angio-Osteogenic Biomaterial for In Vivo Osseointegration and Bone Repair. *Adv. Biol.* **2023**, e2300039. [[CrossRef](#)]

18. Martins, E.; Diogo, G.S.; Pires, R.; Reis, R.L.; Silva, T.H. 3D Biocomposites Comprising Marine Collagen and Silica-Based Materials Inspired on the Composition of Marine Sponge Skeletons Envisaging Bone Tissue Regeneration. *Mar. Drugs* **2022**, *20*, 718. [[CrossRef](#)]
19. Goodarzi, H.; Hashemi-Najafabadi, S.; Baheiraei, N.; Bagheri, F. Preparation and Characterization of Nanocomposite Scaffolds (Collagen/ $\beta$ -TCP/SrO) for Bone Tissue Engineering. *Tissue Eng. Regen. Med.* **2019**, *16*, 237–251. [[CrossRef](#)]
20. Añazco, C.; Riedelsberger, J.; Vega-Montoto, L.; Rojas, A. Exploring the Interplay between Polyphenols and Lysyl Oxidase Enzymes for Maintaining Extracellular Matrix Homeostasis. *Int. J. Mol. Sci.* **2023**, *24*, 10985. [[CrossRef](#)]
21. Tseomashko, N.Y.; Abidova, A.D.; Makhmudov, S.D.; Azimova, S.S.; Aripova, S.F. Evaluation of the biological activity of phyllalbin and rutin, and application in wound dressings. *J. Hum. Univ.* **2021**, *48*, 530–550.
22. Tseomashko, N.E.; Abidova, A.D.; Makhmudov, S.D.; Rakhmanov, A.K. Evaluation of gastroprotective and regenerative properties of flavonoids isolated from buds of *Saphora Japonica* in collagen. *J. Hum. Univ.* **2021**, *48*, 551–561.
23. Kadian, S.; Manik, G.; Das, N.; Nehra, P.; Chauhan, R.P.; Roy, P. Synthesis, characterization and investigation of synergistic antibacterial activity and cell viability of silver-sulfur doped graphene quantum dot (Ag@S-GQDs) nanocomposites. *J. Mater. Chem.* **2020**, *8*, 3028–3037. [[CrossRef](#)]
24. Rai, M.; Yadav, A.; Gade, A. Silver nanoparticles as a new generation of antimicrobials. *Biotechnol. Adv.* **2009**, *27*, 76–83. [[CrossRef](#)]
25. Shrivastava, S.; Bera, T.; Roy, A.; Singh, G.; Ramachandrarao, P.; Dash, D. Characterization of enhanced antibacterial effects of novel silver nanoparticles. *Nanotechnology* **2007**, *18*, 225103. [[CrossRef](#)]
26. Kim, J.S.; Kuk, E.; Yu, K.N.; Kim, J.-H.; Park, S.J.; Lee, H.J.; Kim, S.H.; Park, Y.K.; Park, Y.H.; Hwang, C.-Y.; et al. Antimicrobial effects of silver nanoparticles. *Nanomed. Nanotechnol. Biol. Med.* **2007**, *3*, 95–101. [[CrossRef](#)] [[PubMed](#)]
27. Amiri, N.; Ghaffari, S.; Hassanpour, I.; Chae, T.; Jalili, R.; Taghi Kilani, R.; Ko, F.; Ghahary, A.; Lange, D. Antibacterial Thermosensitive Silver–Hydrogel Nanocomposite Improves Wound Healing. *Gels* **2023**, *9*, 542. [[CrossRef](#)]
28. Albu, M.G.; Vladkova, T.G.; Ivanova, I.A.; Shalaby, A.S.A.; Moskova-Doumanova, V.S.; Staneva, A.D.; Dimitriev, Y.B.; Kostadinova, A.S.; Topouzova-Hristova, T.I. Preparation and Biological Activity of New Collagen Composites, Part I: Collagen/Zinc Titanate Nanocomposites. *Appl. Biochem. Biotechnol.* **2016**, *180*, 177–193. [[CrossRef](#)] [[PubMed](#)]
29. Park, D.; Osuji, C.O.; Kim, J.W. Multi-Compartmentalized Cellulose Macrobead Catalysts for In Situ Organic Reaction in Aqueous Media. *Small Methods* **2023**, *7*, 2201195. [[CrossRef](#)]
30. Prucek, R.; Kvítek, L.; Panáček, A.; Vančurová, L.; Soukupová, J.; Jančík, D.; Zbořil, R. Polyacrylate-assisted synthesis of stable copper nanoparticles and copper(I) oxide nanocubes with high catalytic efficiency. *J. Mater. Chem.* **2009**, *19*, 8463–8469. [[CrossRef](#)]
31. Jinga, S.I.; Isopencu, G.; Stoica-Guzun, A.; Stroescu, M.; Ferdes, M.; Ohreac, B. Silver green synthesis on bacterial cellulose membranes using tannic acid. *Dig. J. Nanomater. Bios.* **2013**, *8*, 1711–1717.
32. Sarkandi, F.A.; Montazer, M.; Harifi, T.; Rad, M.M. Innovative preparation of bacterial cellulose/silver nanocomposite hydrogels: In situ green synthesis, characterization, and antibacterial properties. *J. Appl. Polym. Sci.* **2021**, *138*, 49824. [[CrossRef](#)]
33. Kucińska-Lipka, J.; Gubanska, I.; Janik, H. Bacterial Cellulose in the Field of Wound Healing and Regenerative Medicine of Skin: Recent Trends and Future Perspectives. *Polym. Bull.* **2015**, *72*, 2399–2419. [[CrossRef](#)]
34. Wei, D.; Sun, W.; Qian, W.; Ye, Y.; Ma, X. The synthesis of chitosan-based silver nanoparticles and their antibacterial activity. *Carbohydr. Res.* **2009**, *344*, 2375–2382. [[CrossRef](#)]
35. Twu, Y.-K.; Chen, Y.-W.; Shih, C.-M. Preparation of silver nanoparticles using chitosan suspensions. *Powder Technol.* **2008**, *185*, 251–257. [[CrossRef](#)]
36. Vasil'kov, A.Y.; Abd-Elsalam, K.A.; Olenin, A.Y. Biogenic Silver Nanoparticles: New Trends and Applications. In *Green Synthesis of Silver Nanomaterials*; Abd-Elsalam, K.A., Ed.; Elsevier: Amsterdam, The Netherlands, 2021; pp. 241–281. [[CrossRef](#)]
37. Mikhailov, O.V.; Mikhailova, E.O. Elemental silver nanoparticles: Biosynthesis and bio applications. *Materials* **2019**, *12*, 3177. [[CrossRef](#)] [[PubMed](#)]
38. Ahn, E.-Y.; Jin, H.; Park, Y. Assessing the antioxidant, cytotoxic, apoptotic and wound healing properties of silver nanoparticles green-synthesized by plant extracts. *Mater. Sci. Eng. C* **2019**, *101*, 204–216. [[CrossRef](#)]
39. Hamed, S.; Shojaosadati, S.A. Rapid and green synthesis of silver nanoparticles using *Diospyros lotus* extract: Evaluation of their biological and catalytic activities. *Polyhedron* **2019**, *171*, 172–180. [[CrossRef](#)]
40. Hernández-Morales, L.; Espinoza-Gómez, H.; Flores-López, L.Z.; Sotelo-Barrera, E.L.; Núñez-Rivera, A.; Cadena-Nava, R.D.; Alonso-Núñez, G.; Espinoza, K.A. Study of the green synthesis of silver nanoparticles using a natural extract of dark or white *Salvia hispanica* L. seeds and their antibacterial application. *Appl. Surf. Sci.* **2019**, *489*, 952–961. [[CrossRef](#)]
41. Küp, F.Ö.; Çoşkunçay, S.; Duman, F. Biosynthesis of silver nanoparticles using leaf extract of *Aesculus hippocastanum* (horse chestnut): Evaluation of their antibacterial, antioxidant and drug release system activities. *Mater. Sci. Eng. C* **2020**, *107*, 110207. [[CrossRef](#)]
42. Tseomashko, N.E.; Rai, M.; Vasil'kov, A.Y. New hybrid materials for wound cover dressings. In *Bio-Polymer-Based Nano Films*; Rai, M., Dos Santos, C.A., Eds.; Elsevier Inc.: New York, NY, USA, 2021; pp. 203–246. [[CrossRef](#)]
43. Barbaro, D.; Di Bari, L.; Gandin, V.; Evangelisti, C.; Vitulli, G.; Schiavi, E.; Marzano, C.; Ferretti, A.M.; Salvadori, P. Glucose-coated superparamagnetic iron oxide nanoparticles prepared by metal vapour synthesis are electively internalized in a pancreatic adenocarcinoma cell line expressing GLUT1 transporter. *PLoS ONE* **2015**, *10*, e0123159. [[CrossRef](#)] [[PubMed](#)]
44. Cárdenas-Triviño, G.; Cruzat-Contreras, C. Study of Aggregation of Gold Nanoparticles in Chitosan. *J. Clust. Sci.* **2018**, *29*, 1081–1088. [[CrossRef](#)]

45. Vasil'kov, A.; Voronova, A.; Batsalova, T.; Moten, D.; Naumkin, A.; Shtykova, E.; Volkov, V.; Teneva, I.; Dzhambazov, B. Evolution of gold and iron oxide nanoparticles in conjugates with methotrexate: Synthesis and anticancer effects. *Materials* **2023**, *16*, 3238. [CrossRef] [PubMed]
46. Vasil'kov, A.; Butenko, I.; Naumkin, A.; Voronova, A.; Golub, A.; Buzin, M.; Shtykova, E.; Volkov, V.; Sadykova, V. Hybrid Silver-Containing Materials Based on Various Forms of Bacterial Cellulose: Synthesis, Structure, and Biological Activity. *Int. J. Mol. Sci.* **2023**, *24*, 7667. [CrossRef] [PubMed]
47. Jose, D.; Jagirdar, B.R. Au@Pd core-shell nanoparticles through digestive ripening. *J. Phys. Chem. C* **2008**, *112*, 10089–10094. [CrossRef]
48. Bhaskar, S.P.; Jagirdar, B.R. Digestive ripening: A synthetic method par excellence for core-shell, alloy, and composite nanostructured materials. *J. Chem. Sci.* **2012**, *124*, 1175–1180. [CrossRef]
49. Balerna, A.; Evangelisti, C.; Psaro, R.; Fusini, G.; Carpita, A. Structural characterization of bimetallic Pd-Cu vapor derived catalysts. *J. Phys. Conf. Ser.* **2016**, *712*, 12057. [CrossRef]
50. Abd-El Salam, K.A.; Alghuthaymi, M.A.; Shami, A.; Rubina, M.S.; Abramchuk, S.S.; Shtykova, E.V.; Vasil'kov, A.Y. Copper-Chitosan Nanocomposite Hydrogels against Aflatoxigenic *Aspergillus flavus* from Dairy Cattle Feed. *J. Fungi* **2020**, *6*, 112. [CrossRef]
51. Vasil'kov, A.Y.; Migulin, D.A.; Muzalevskiy, V.M.; Naumkin, A.V.; Pereyaslvtsev, A.Y.; Zubavichus, Y.V.; Nenajdenko, V.G.; Muzafarov, A.M. Copper-containing polymethylsilsequioxane nanocomposites in catalytic olefination reaction. *Mend. Commun.* **2022**, *32*, 478–481. [CrossRef]
52. Rubina, M.S.; Said-Galiev, E.E.; Naumkin, A.V.; Shulenina, A.V.; Belyakova, O.A.; Vasil'kov, A. Preparation and characterization of biomedical collagen–chitosan scaffolds with entrapped ibuprofen and silver nanoparticles. *Polym. Eng. Sci.* **2019**, *59*, 2479–2487. [CrossRef]
53. Vasil'kov, A.; Migulin, D.; Naumkin, A.; Volkov, I.; Butenko, I.; Golub, A.; Sadykova, V.; Muzafarov, A. Hybrid Materials with Antimicrobial Properties Based on Hyperbranched Polyaminopropylalkoxysiloxanes Embedded with Ag Nanoparticles. *Pharmaceutics* **2023**, *15*, 809. [CrossRef] [PubMed]
54. Rubina, M.S.; Elmanovich, I.V.; Shulenina, A.V.; Peters, G.S.; Svetogorov, R.D.; Egorov, A.A.; Vasil'kov, A.Y. Chitosan aerogel containing silver nanoparticles: From metal-chitosan powder to porous material. *Polym. Test.* **2020**, *86*, 106481. [CrossRef]
55. Vasil'kov, A.; Rubina, M.; Naumkin, A.; Buzin, M.; Dorovatovskii, P.; Peters, G.; Zubavichus, Y. Cellulose-Based Hydrogels and Aerogels Embedded with Silver Nanoparticles: Preparation and Characterization. *Gels* **2021**, *7*, 82. [CrossRef]
56. Vasil'kov, A.; Rubina, M.; Naumkin, A.; Belyakova, O.; Zubavichus, Y.; Maksimov, Y.; Imshennik, V. Metal-containing systems based on chitosan and collagen-chitosan composite. *Russ. Chem. Bull.* **2015**, *64*, 1663–1670. [CrossRef]
57. Rubina, M.S.; Kamitov, E.; Zubavichus, Y.; Peters, G.; Naumkin, A.; Suzer, S.; Vasil'kov, A. Collagen-chitosan scaffold modified with Au and Ag nanoparticles: Synthesis and structure. *Appl. Surf. Sci.* **2016**, *366*, 365–371. [CrossRef]
58. Kaulambaeva, M.Z.; Nurmukhambetova, A.B.; Aidarova, M.M.; Akhmetsadykov, N.N.; Khusainov, D.M. Method for Obtaining Collagen. Patent (19) KZ (13) A4 (11) 30528, 2015. Available online: <https://kzpatents.com/2-ip30528-sposob-polucheniya-kollagena.html> (accessed on 30 June 2023).
59. Konarev, P.V.; Volkov, V.V.; Sokolova, A.V.; Koch, M.H.J.; Svergun, D.I. PRIMUS—A Windows-PC based system for small-angle scattering data analysis. *J. Appl. Cryst.* **2003**, *36*, 1277–1282. [CrossRef]
60. Manalastas-Cantos, K.; Konarev, P.V.; Hajizadeh, N.R.; Kikhney, A.G.; Petoukhov, M.V.; Molodenskiy, D.S.; Panjkovich, A.; Mertens, H.D.T.; Gruzinov, A.; Borges, C.; et al. ATSAS 3.0: Expanded functionality and new tools for small-angle scattering data analysis. *J. Appl. Cryst.* **2021**, *54*, 343–355. [CrossRef] [PubMed]
61. Feigin, L.A.; Svergun, D.I. *Structure Analysis by Small-Angle X-ray and Neutron Scattering*; Plenum Press: New York, NY, USA, 1987; 176p.
62. Svergun, D.I. Determination of the regularization parameter in indirect-transform methods using perceptual criteria. *J. Appl. Cryst.* **1992**, *25*, 495–503. [CrossRef]
63. Beamson, G.; Briggs, D. *High Resolution XPS of Organic Polymers: The Scienta ESCA300 Database*; Wiley: Chichester, UK, 1992.
64. Abidova, A.D.; Tseomashko, N.E.; Aripova, S.F. Obtaining components for wound coverings and assessing their biological activity. *Univers. Chem. Biol. Electron. Sci. J.* **2019**, *11*, 65. Available online: <http://7universum.com/ru/nature/archive/item/7904> (accessed on 30 June 2023).
65. Vidal, A.R.; Duarte, L.P.; Schmidt, M.M.; Cansian, R.L.; Fernandes, I.A.; de Oliveira, M.R.; Demiate, I.M.; Dornelles, R.C.P. Extraction and characterization of collagen from sheep slaughter by-products. *Waste Manag.* **2020**, *102*, 838–846. [CrossRef]
66. Wu, W.; Wang, R.; Chang, H.; Zhong, N.; Zhang, T.; Wang, K.; Ren, N.; Ho, S.-H. Rational electron tuning of magnetic biochar via N, S co-doping for intense tetracycline degradation: Efficiency improvement and toxicity alleviation. *Chem. Eng. J.* **2023**, *458*, 141470. [CrossRef]
67. Cucos, A.; Budrugaec, P. Simultaneous TG/DTG–DSC–FTIR characterization of collagen in inert and oxidative atmospheres. *J. Therm. Anal. Calorim.* **2014**, *115*, 2079–2087. [CrossRef]
68. Owczarzy, A.; Kurasiński, R.; Kulig, K.; Rogóż, W.; Szkudlarek, A.; Maciążek-Jurczyk, M. Collagen—Structure, properties and application. *Eng. Biomater.* **2020**, *156*, 17–23. [CrossRef]
69. Gentile, P.; McColgan-Bannon, K.; Gianone, N.C.; Sefat, F.; Dalgarno, K.; Ferreira, A.M. Biosynthetic PCL-graft-Collagen Bulk Material for Tissue Engineering Applications. *Materials* **2017**, *10*, 693. [CrossRef] [PubMed]

70. Sionkowska, A.; Wisniewski, M.; Kaczmarek, H.; Skopinska, J.; Chevallier, P.; Mantovani, D.; Lazare, S.; Tokarev, V. The influence of UV irradiation on surface composition of collagen/PVP blended films. *Appl. Surf. Sci.* **2006**, *253*, 1970–1977. [[CrossRef](#)]
71. Gengenbach, T.R.; Major, G.H.; Linford, M.R.; Easton, C.D. Practical guides for X-ray photoelectron spectroscopy (XPS): Interpreting the carbon 1 s spectrum. *J. Vac. Sci. Technol. A* **2021**, *39*, 13204. [[CrossRef](#)]
72. Zambonin, G.; Losito, I.; Triffitt, J.T.; Zambonin, C.G. Detection of collagen synthesis by human osteoblasts on a tricalcium phosphate hydroxyapatite: An X-ray photoelectron spectroscopy investigation. *J. Biomed. Mater. Res.* **2000**, *49*, 120–126. [[CrossRef](#)]
73. Boronin, A.I.; Koscheev, S.V.; Zhidomirov, G.M. XPS and UPS study of oxygen states on silver. *J. Electron Spectrosc. Relat. Phenom.* **1998**, *96*, 43–51. [[CrossRef](#)]
74. Hoflund, G.B.; Weaver, J.F.; Epling, W.S. Ag Foil by XPS. *Surf. Sci. Spectra* **1994**, *3*, 151–156. [[CrossRef](#)]
75. Hoflund, G.B.; Weaver, J.F.; Epling, W.S. Ag<sub>2</sub>O XPS Spectra. *Surf. Sci. Spectra* **1994**, *3*, 157–162. [[CrossRef](#)]
76. Hoflund, G.B.; Weaver, J.F.; Epling, W.S. AgO XPS Spectra. *Surf. Sci. Spectra* **1994**, *3*, 163–168. [[CrossRef](#)]
77. Kaushik, V.K. XPS core level spectra and Auger parameters for some silver compounds. *J. Electron. Spectrosc. Relat. Phenom.* **1991**, *56*, 273–277. [[CrossRef](#)]

**Disclaimer/Publisher’s Note:** The statements, opinions and data contained in all publications are solely those of the individual author(s) and contributor(s) and not of MDPI and/or the editor(s). MDPI and/or the editor(s) disclaim responsibility for any injury to people or property resulting from any ideas, methods, instructions or products referred to in the content.